Nortek Technical Note No.: *011*
Title: *Aquadopp and Vector wave measurement near Scripps Pier*
Last Edited: *November 19, 1999*
Authors: *Lee Gordon, NortekUSA & Linden Clarke, Scripps Institution of Oceanography*
No. of Pages: *10*

Aquadopp and Vector wave measurement near Scripps Pier

This report summarizes data collected from the near-shore and surf zone, using two Doppler current meters, the Aquadopp and the Vector. The Aquadopp was deployed near the end of Scripps Pier and the Vector was deployed in the nearby surf zone. Data were collected in three short deployments during July and October 1999. Our objective was to evaluate the use of these instruments to study wave processes and to try out simple deployment methods.

We conclude that both instruments are suitable for observation of wave directional spectra.

Instruments

The Aquadopp is a standard, general-purpose Doppler current meter, and the Vector is a bistatic Doppler sensor, also called an Acoustic Doppler Velocimeter (ADV). An ADV measures three velocity components with high resolution in a single, small volume of water. Both sensors are small relative to other equivalent high performance Doppler instruments. Their small size makes them relatively easy to deploy, which means they can be used in a wider range of investigations. Figure 1 shows a picture of the Aquadopp, and Figure 2 diagrams a Vector probe.

The Vector can sample at rates up to 64 Hz to observe rapid processes such as waves and turbulence, and its low drift rates mean it can measure low frequency currents as well. Its small, well-defined measurement volume, small physical size and rapid sampling are appropriate for deployment in shallow water sites such as the surf zone. Burst mode sampling facilitates longer deployments.

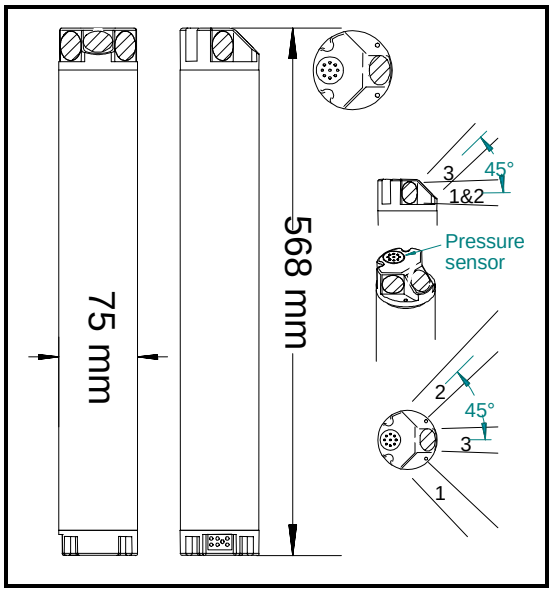

Figure 1. Aquadopp current meter.

The Aquadopp is a general-purpose current meter designed for long-term deployment in the ocean, estuaries and lakes. It observes water level (via pressure), water temperature and currents. It is able to sample wave velocity and pressure at rates up to 1 Hz, but its larger measurement volume means it requires greater water depth than the Vector.

The Aquadopp is designed to record long-term low frequency currents, but a special burst mode enables it to collect wave time series at long intervals (i.e. 3-6 hours) while it collects mean current data at shorter intervals. The Aquadopp's versatility is particularly well suited for organizations with widely varying requirements.

Details of these systems are available at: www.nortek-as.com and www.NortekUSA.com.

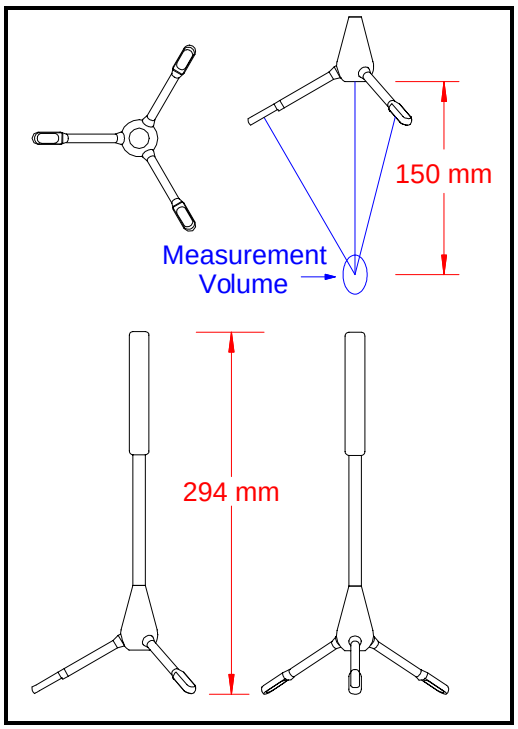

Figure 2. Vector Current Meter cable probe. The Vector pressure case is approximately the same size as an Aquadopp, and the probe is attached to the electronics by a 5 mm x 2 m cable.

Figure 3. Map showing three deployment locations. A is the location of the Aquadopp deployment, and the two Vector deployments were at B and C.

Figure 4. Vector installation.

Installation

One objective for these measurements was to install the instruments with minimal manpower. Both were installed on pipes jetted into the sand. The Vector was installed in the surf zone for short deployments on July 31 and October 25, 1999, and the Aquadopp was installed overnight at the end of Scripps Pier starting on October 8, 1999 (Figure 3).

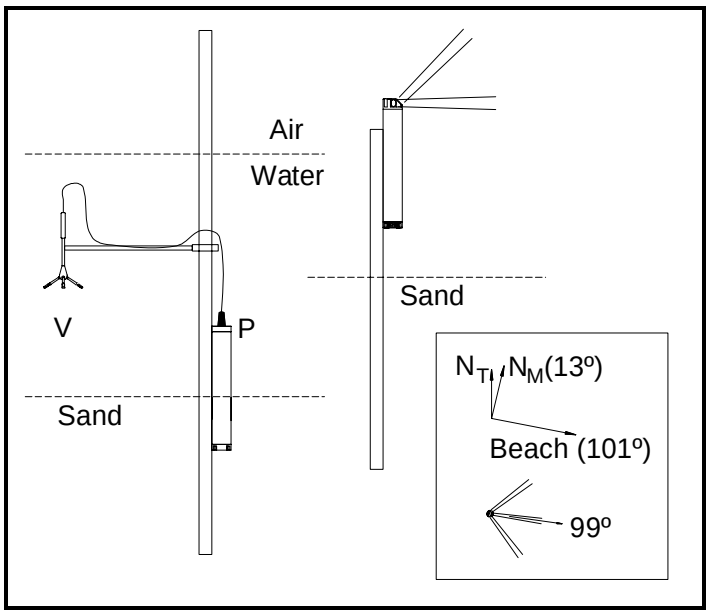

Figure 5. Vector (left) and Aquadopp (right) mounts. The Vector's sensing locations are shown with letters for velocity (V) and pressure (P). The inset at the right shows directions for true north (N_T), magnetic north (N_M), normal to the beach and the Aquadopp orientation. Because the beach is relatively straight, the angles at the bottom right apply for all three measurements.

We installed the Vector in 0.6-0.9 m deep water in the surf zone. Installation in the surf zone was a one-man job (Figure 4). The Vector was mounted on a pole with an arm to hold the probe (Figure 5). The pole was jetted into the sand, partially burying the pressure case—our intent was to obtain pressure and velocity measurements from the same depth. Jetting was accomplished with a scuba tank and a thin metal tube, which injected air to fluidize the sand. Two scuba divers deployed the Aquadopp in 8 m water depth using much the same approach. In all cases, tilt was 3° or less.

Observations

Comparison wave spectra from the CDIP program were obtained via the Internet (cdip.ucsd.edu). These spectra were computed hourly using 34-minute pressure time series from a sensor mounted at the end of Scripps Pier. There are no nearby directional data available for comparison.

Near-shore observations

The Aquadopp collected velocity and pressure data with a 1-s interval continuously for 13.7 hours. Data recording stopped when its 2 MB internal recorder became full. Figure 6 shows three time series from the Aquadopp observations. The top panels show low-passed time series and pressure for the entire data set, smoothed into 5-minute intervals. The middle panels show a 600-s interval of wave data and the bottom panels show a 70-s detail taken from within the middle time series.

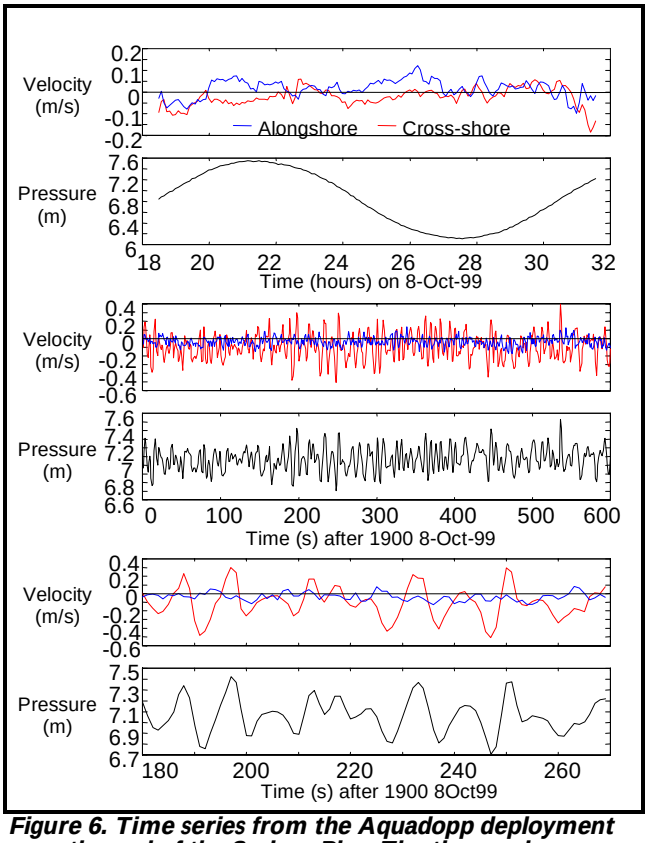

Figure 6. Time series from the Aquadopp deployment near the end of the Scripps Pier. The time series use the same color coding throughout the figure.

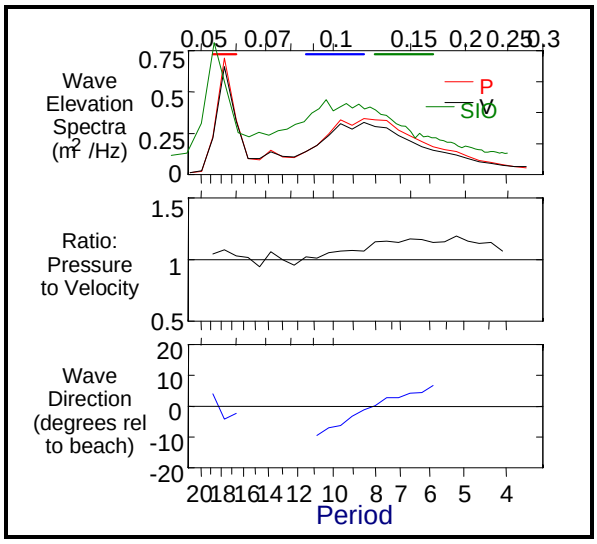

Figure 7. Surface wave elevation spectra of Aquadopp pressure (P) and velocity (V) and from the Scripps Pier (SIO) pressure sensor. The different peak frequencies are a function of the processing (different averaging intervals) and are not real (see Appendix A). The bars at the top of the panel indicate three frequency bands used for Figure 8. The middle panel shows the ratio of the Aquadopp pressure and velocity spectra and the bottom panel shows wave direction computed in the energetic parts of the spectrum.

The Aquadopp was oriented within a few degrees of normal to the shoreline, and the data were rotated into along-shore and cross-shore components. These time series show a surface tidal range of around 1.5 m and along- and cross-shore currents on the order of 0.1 m/s. Wave frequency velocities were oriented toward the beach and the pressure and velocity signals were coherent with one another.

Figure 7 compares wave elevation power spectra from the Aquadopp and from the Scripps Pier pressure sensor. Appendix A compares the Aquadopp and Scripps Pier pressure measurements in more detail. The Aquadopp pressure and velocity spectra were transformed to surface elevation spectra using equations in Appendix B. The Aquadopp and Scripps Pier spectra are averages from roughly the same time interval. The spectra consist of two well-separated peaks, a relatively narrow swell peak at around 18 s, and a broader peak covering 6-12 s periods.

All three spectra compare well with one another. The middle panel shows the ratio of the Aquadopp

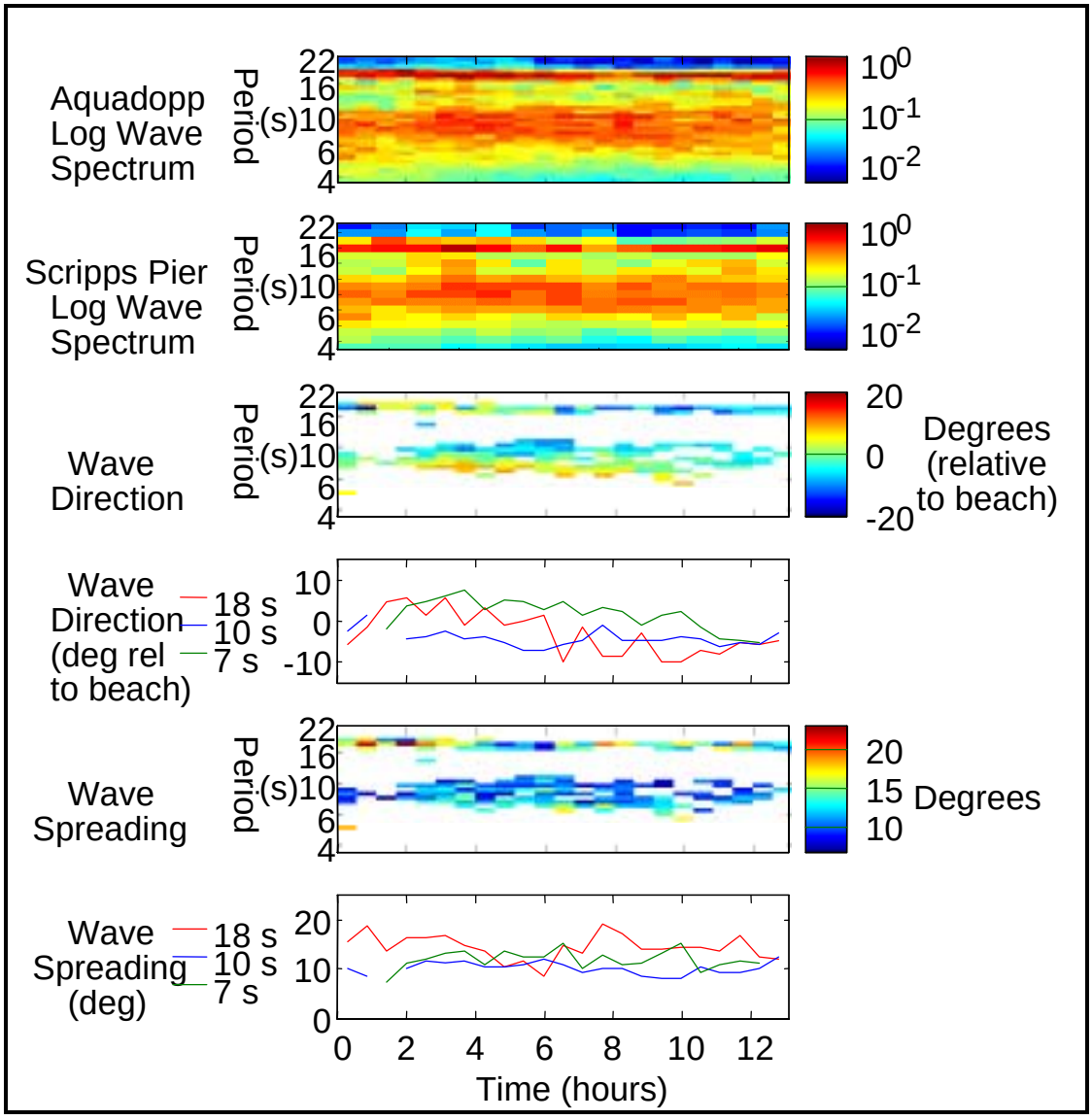

Figure 8. Top two panels are contour plots of spectra. The first uses the average of the Aquadopp velocity and pressure surface elevation spectra. The second uses the data from Scripps Pier. The middle two panels show wave direction in the energetic parts of the spectra and the bottom shows wave spreading. The three wave direction and wave spreading time series correspond to frequency bands defined in the top panel of Figure 7.

pressure and velocity spectra. Ideally the ratio should be unity—the way that the ratio grows with frequency suggests a correction error rather than an error in either the velocity or pressure measurement. The bottom panel shows wave direction computed using equations in Appendix B.

Figure 8 shows wave spectra and directional parameters in more detail. The top panel shows how the Aquadopp wave spectrum evolves over the 13-hour measurement period, and the second panel shows the same for the Scripps Pier data—the two look much alike.

The third and fourth panels show wave direction, first as color contour plots, then as time series. The color contour plots show that, at least in the energetic parts of the spectrum, the wave direction smoothly varies with time and frequency. The three time series show wave directions for three frequency bands defined in Figure 7. The direction angles fall with time, which corresponds to waves coming from wind systems tracking northward. The bottom two panels show estimated wave spreading.

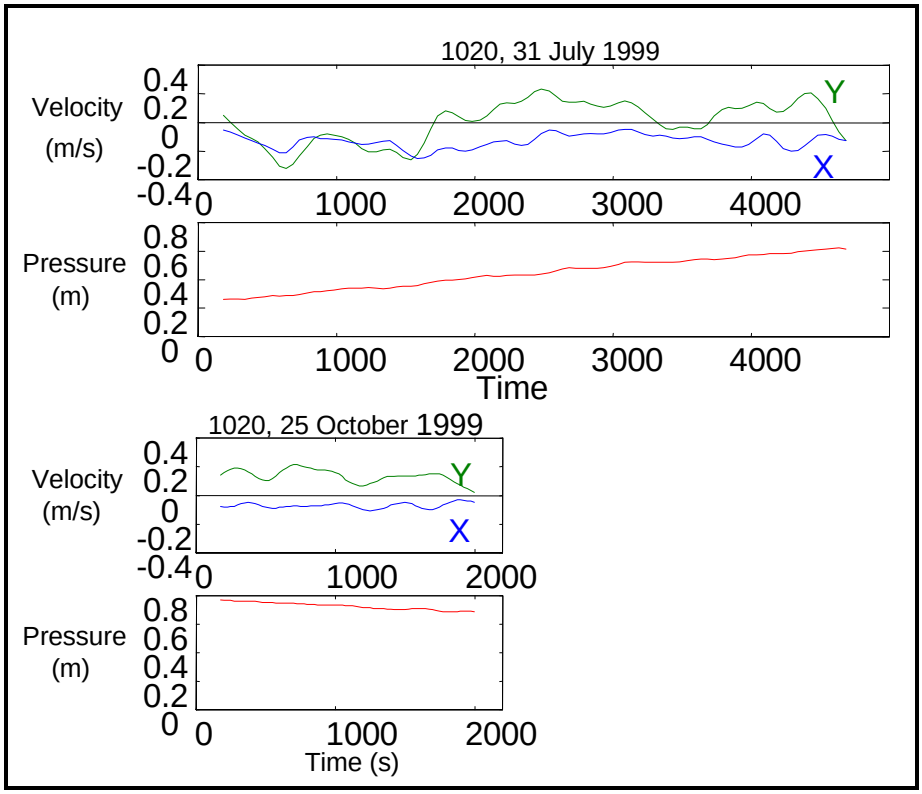

Figure 9. Low-passed time series from two Vector deployments in the surf zone. The X-component is normal to the beach, positive east, and the Y-component is parallel to the beach, positive north. The varying pressure is the result of changing tides.

Surf-zone observations

We deployed the Vector for two short deployments. The first (31 July) collected data at 4 Hz for 81 minutes and the second (25 October) collected 8 Hz data for 37 minutes. Figure 9 shows low-passed currents during both deployments.

Figure 10 shows time series of waves and wave groups. The wave velocities were perpendicular to the shore and characterized by relatively short surges, corresponding to passages of wave bores. The velocity and pressure signals are well correlated.

Figure 11 shows spectra from both deployments. The velocity and pressure spectra were scaled to surface elevation spectra using equations in Appendix B, and direction was computed using equations also in Appendix B. The ratio "P/V" is the ratio of pressure and velocity power spectra, each scaled to surface elevation spectra using linear theory; the ratio should be unity under linear waves.

Waves were larger during the July deployment, but the surf-zone motions were comparable in magnitude for both deployments. The spectra can be divided at roughly 0.05 Hz (20 s period). Wave dynamics dominates above this cutoff: the P/V ratio is around 1.0, and the computed wave direction is onshore. The large P/V ratio at 0.075 Hz (13 s) in the October deployment could result from wave reflection from the beach. Below the cutoff, the P/V and direction curves look similar for the two deployments. This suggests that similar low-frequency dynamics applied for both deployments.

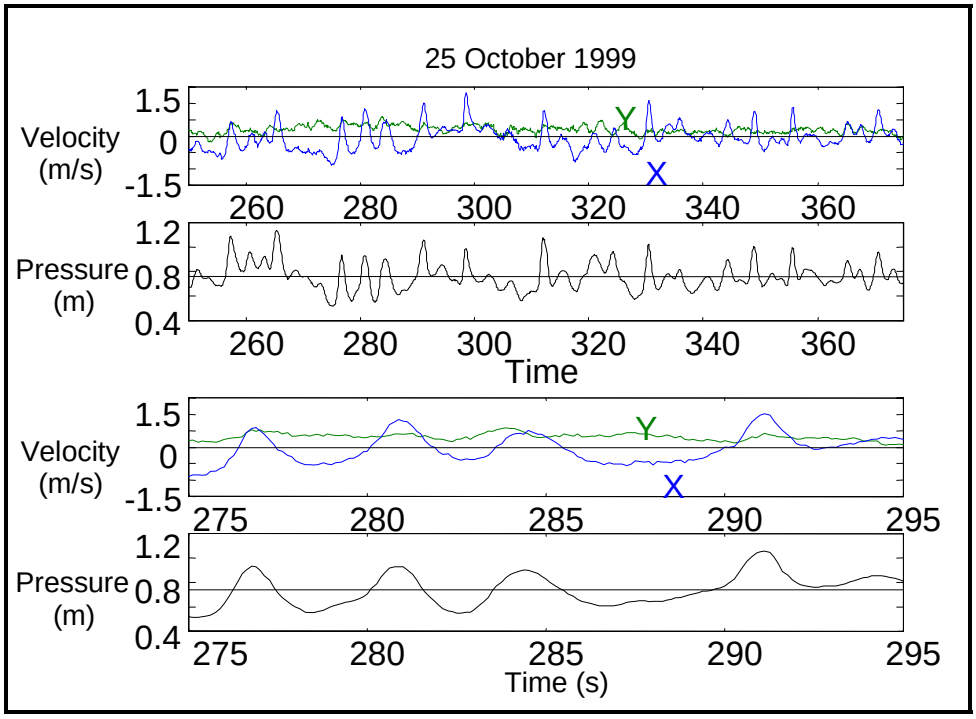

Figure 10. Raw velocity and pressure time series observed by the Vector.

The X-component is normal to the beach, positive east, and the Y-component is parallel to the beach, positive north.

The lower panels show a detail of a segment from the upper panels.

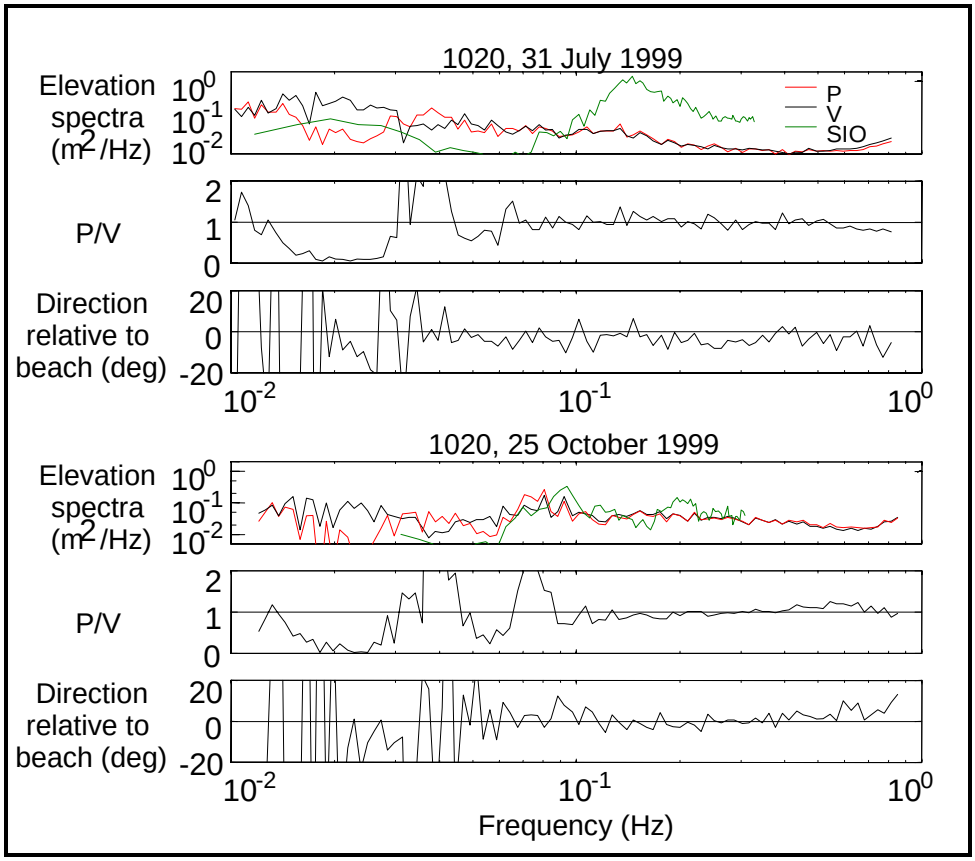

Figure 11. Spectra from the two Vector surf-zone deployments.

Elevation spectra are based on velocity (V) and pressure (P) from the Vector, and data from the Scripps pier (SIO), outside the surf zone. "P/V" is the ratio of the Vector pressure and velocity spectra.

Appendix A. Comparison of Aquadopp and Scripps Pier pressure sensors.

The Aquadopp was within about 10 m of the end of the Scripps Pier, but we do not know the exact distance and orientation. The two signals nevertheless correspond well with one another.
For detailed comparison, we obtained Scripps Pier time pressure series, courtesy of David Castel. The Scripps Pier pressure sensor is a Paroscientific quartz sensor, sampled at 1 Hz. Because the two signals were not synchronized, it was necessary to do so visually by comparison of individual time series. Figure 12 shows the two signals plotted on top of one another. The close relationship in the bottom panel of Figure 12 was characteristic of the entire 9-hour time series.

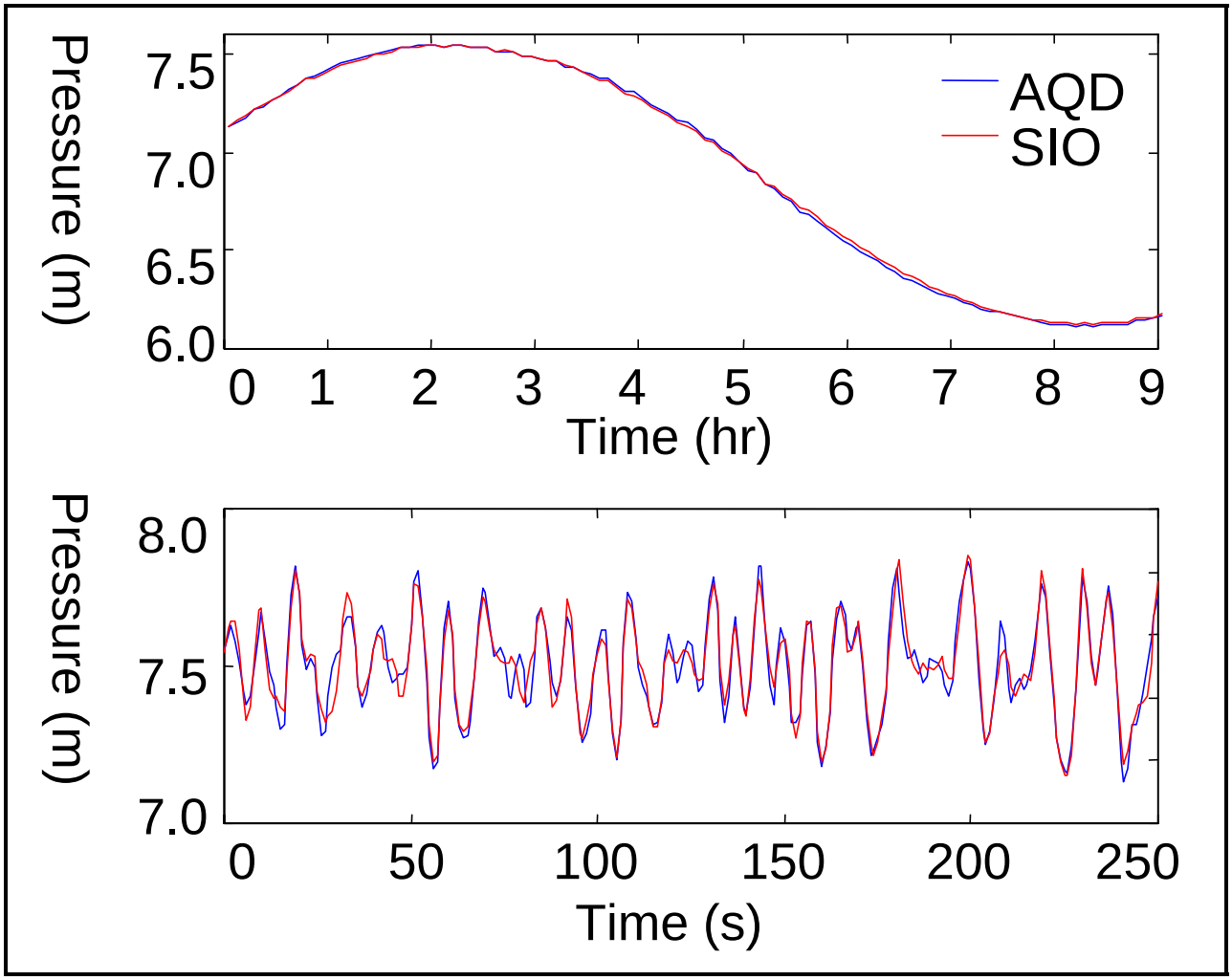

Figure 12. Time series comparison of Aquadopp and Scripps Pier pressure signals. Top: low-passed pressure. Bottom: unfiltered time series (sampled at 1 Hz) from around 3 hours after the beginning. To facilitate comparison, the time series were offset both in time and pressure to obtain the best possible visual correlation.

Figure 13 compares the two signals spectrally. The overall spectra appear identical and are coherent up to around 0.25 Hz. At frequencies below 0.05 Hz, the average Aquadopp pressure power spectrum is about 0.8% greater than the Scripps Pier power spectrum. In the wave band (0.05-0.3 Hz), the Aquadopp pressure signal is about 5% higher. The Aquadopp was deployed at an approximate depth of 6.8 m and the Scripps Pier pressure sensor was at a mean depth of 6.6 m. This difference in depth would cause a difference in spectra (see Appendix B for the equation), but the difference appears not to be significant where the pressure spectra are above their noise levels. Given our uncertainty in the

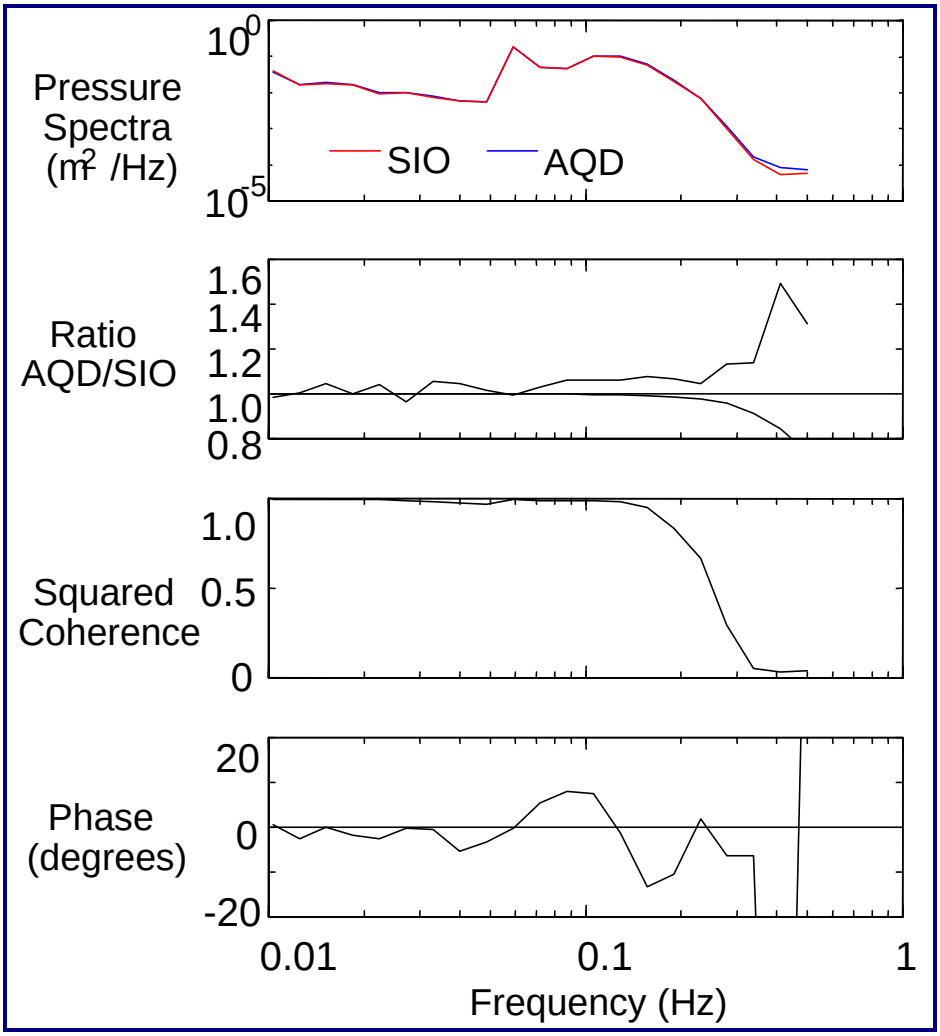

Figure 13. Comparison of Aquadopp and Scripps Pier power spectra. The top panel shows the both Aquadopp and Scripps Pier pressure spectra, and the second panel shows the ratio of the two. The smooth line curving downward on the second panel is the predicted ratio given their approximate depths. The predicted ratio becomes significant above around 0.3 Hz, but both pressure signals are largely noise above 0.3 Hz. The third panel shows the coherence between the two signals—squared coherence falls to 0.5 at 0.25 Hz. The fourth panel shows the coherence phase difference between the two sensors.

actual relative depths of the Aquadopp and Scripps Pier pressure sensors, we should not put too much stock in the magnitude of the predicted ratio, but the frequency behavior is worth noting.
Above about 0.3 Hz, the pressure spectra flatten out, suggesting a noise floor. If we assumed that this noise floor represented a white noise across the full spectrum, the rms uncertainties would be around 9 mm for the Aquadopp and 7 mm for the Scripps Pier pressure. However, these noise levels are probably not instrumental uncertainties. The Aquadopp's uncertainty should be around 1-2 mm and the Paroscientific pressure sensor's uncertainty should be much less than 1 mm. Corresponding noise levels are far below the observed spectral noise levels. In addition, the fact that the observed noise levels are roughly the same, even though the instrumental noise levels should be substantially different, suggests another source for the observed noise.

Herbers and Guza (1991, 1992 and 1994) describe nonlinear motions that could produce noise levels we observed. Surface waves attenuate rapidly with depth, decaying to near-nothingness within just a few wavelengths of the ocean surface. Yet observable wave frequency motions are ubiquitous in the ocean, even at abyssal depths. Needless to say, these motions do not scale like surface waves, but the motions

can produce real pressure fluctuations that stand above both instrumental noise and linear surface wave motions. A corollary to this fact is that these motions limit the value of improving pressure sensor resolution. When these "not-linear-surface-wave" motions exceed instrumental uncertainty, then improved pressure sensors do little to improve the quality of surface wave spectra.

Appendix B. Equations

Conversion of pressure (C_{pp}) and velocity (C_{uu}) power spectra to surface elevation power spectra uses the following equations:

$$C_{\eta\eta p} = \left[\frac{\cosh kh}{\cosh k(h+z)}\right]^2 \frac{C_{pp}}{\rho^2 g^2} \quad (1)$$

and

$$C_{\eta\eta u} = \left[\frac{\sinh kh}{\cosh k(h+z)}\right]^2 \frac{C_{uu}}{\sigma^2} \quad (2)$$

where $C_{\eta\eta p}$ and $C_{\eta\eta u}$ represent surface elevation (η) spectra based on pressure and velocity, k is wavenumber, h is mean water level relative to the seabed, z is the vertical distance relative to the mean water level (positive up), σ is frequency, ρ is water density and g is gravity.

The ratio R of power spectra from nearby pressure sensors is:

$$R = \left[\frac{\cosh k(h+z_1)}{\cosh k(h+z_2)}\right]^2 \quad (3)$$

where z_1 and z_2 are depths of the two sensors. Wavenumber and frequency are related according to the dispersion relation:

$$\sigma^2 = gk \tanh kh \quad (4)$$

Direction D is computed using

$$D = \text{atan2}\,(C_{px}, C_{py}) \quad (5)$$

where atan2 is a 4-quadrant arctangent, and C_{px} and C_{py} are the real parts of the pressure-velocity cross-spectra for the x and y velocity components, respectively.
Wave spreading S is computed using

$$S = \text{atan}\left[\frac{\text{real}(2C'_{xy})}{C'_{xx} - C'_{yy}}\right] \quad (5)$$

where C'_{xy}, C'_{xx}, and C'_{yy} are the cross- and co-spectra of the x and y velocity components, after the velocities have been rotated into the dominant wave direction. The co-spectrum is the power spectrum.

References

1. Wave direction:

Herbers, T. H. C., S. Elgar and R. T. Guza, Directional spreading of waves in the nearshore, *J. Geophys. Res.*, **104**(4), 7683-7693,1999.

Kuik, A. J., G. Ph. van Vledder and L. H. Holthuijsen, A method for the routine analysis of pitch-and-roll buoy wave data, *J. Phys. Oceanogr.,* **18**, 1020-1034, 1988.

2. "Not-linear-surface-wave" motions:

Herbers, T. H. C., and R. T. Guza, Wind wave nonlinearity observed at the sea floor, Part I: Forced wave energy, *J. Phys. Oceanogr*., **21**(12), 1740-1761, 1991.

Herbers, T. H. C., and R. T. Guza, Wind-wave nonlinearity observed at the sea floor, Part II: Wavenumbers and third-order statistics, *J. Phys. Oceanogr*., **22**(5), 489-504, 1992.

Herbers, T. H. C., and R. T. Guza, Nonlinear wave interactions and high-frequency sea floor pressure, *J. Geophys. Res.,* **99**(C5), 10035-10048, 1994.